ISSN1027-5495. Functional Materials, 32, No.1 (2025), p. 97-107
doi:http://dx.doi.org/10.15407/fm32.01.97 © 2025 — STC "Institute for Single Crystals"

Application of cellulose nanofibrils in polyvinyl alcohol composite films

Linjuan Duan, Chunxia Chen, Xuan Hou, Bei Liu

Yuncheng Vocational and Technical University , Shanxi, Yuncheng 0443000, China

Received December 5, 2024

Fenton cellulose nanofibrils (F-CNF) were prepared by Fenton oxidation with the followed homogenization and then F-CNF /PVA composite films with the F-CNF additives from 1% to 20% were prepared by solution casting method. Scanning electron microscopy (SEM), confocal laser scanning microscope (CLSM), Fourier transform infrared spectroscopy (FTIR), universal tensile testing machine, swelling property detection, thermogravimetric analysis and soil burial degradation rate test were used to characterize the microstructure, chemical structure, mechanical properties, hygroscopicity, thermal stability and biodegradability of the composites. The results showed that a large number of hydrogen bonds were formed between F-CNF and PVA molecules and an acetal reaction occurred. F-CNF can be uniformly dispersed in PVA matrix, and both have good interfacial compatibility. After the addition of F-CNF, the tensile strength and elastic modulus of the composite films were significantly improved, the water absorption of the composite material was reduced, and its thermal stability was improved. When the amount of F-CNF was 15%, the tensile strength and Young's modulus of the composite films were 65.27 MPa and 1460.32 MPa, respectively, which were 217.77% and 830.69% higher than those of pure PVA.
Keywords: Cellulose nanofibrils; Polyvinyl alcohol; Composite films; Fenton oxidation

Застосування нанофібрил целюлози в композитних плівках з полівінілового спирту. *Linjuan Duan, Chunxia Chen, Xuan Hou, Bei Liu*

Нанофібрили целюлози Фентона (F-CNF) були отримані методом окислення Фентона з наступною гомогенізацією, а потім методом заливки розчину були виготовлені композитні плівки F-CNF/PVA з кількістю добавки F-CNF в діапазоні від 1% до 20%. Скануюча електронна мікроскопія (SEM), конфокальний лазерний скануючий мікроскоп (CLSM), інфрачервона спектроскопія з перетворенням Фур'є (FTIR), універсальна машина для випробувань на розтяг, виявлення властивостей набухання, термогравіметричний аналіз і тест на швидкість деградації заглибленості в ґрунт використовувалися для характеристики мікроструктури, хімічної структури, механічних властивостей, гідроскопічності, термічної стабільності та здатності до біологічного розкладання композитів. Результати показали, що між молекулами F-CNF і PVA утворилася велика кількість водневих зв'язків і відбулася ацетальна реакція. F-CNF може бути рівномірно диспергований у PVA матриці, і обидва мають хорошу міжфазну сумісність. Після додавання F-CNF міцність на розрив і модуль пружності композитних плівок були значно покращені, водопоглинання композитного матеріалу зменшилося, а його термічна стабільність була покращена. Коли кількість F-CNF становила 15%, міцність на розрив і модуль Юнга композитних плівок становили 65,27 МПа і 1460,32 МПа відповідно, що було на 217,77% і 830,69% вище, ніж у чистого ПВС.

1. Introduction

Cellulose nanofibers (CNF) have the characteristics of high strength, high aspect ratio, low thermal expansion coefficient, and biodegradability, and have great potential for application in the field of polymer green reinforcement fillers [1-3]. Compared with CNC, its interwoven three-dimensional network structure can better transmit and disperse loads, endowing materials with certain strength and toughness [4-6]. In recent years, extracting CNF from

biomass resources and utilizing its performance advantages different from CNC to prepare polymer nanocomposites has become a research hotspot in the field of nanocellulose reinforcement. Compared with traditional CNF preparation technology, the Fenton oxidation technology based on microreactor principle with catalyst preloading significantly increases the reaction concentration, avoids the use of toxic and harmful chemicals [7–11], and effectively promotes the large-scale production and industrial utilization of CNF.

Polyvinyl alcohol (PVA), as a polyhydroxy water-soluble polymer, has good film-forming and transparency properties, is easy to process, biodegradable, and has good biocompatibility. It is widely used in textile, food, packaging, tissue engineering, and other fields [12–13]. However, PVA has poor mechanical properties and water resistance, and its comprehensive performance significantly decreases after moisture absorption, which limits its application in the field of high-performance materials. Exploring and developing PVA green composite materials with excellent comprehensive performance remains a major challenge in the field of composite materials.

In this study, Fenton cellulose nanofibers (F-CNF) were prepared using a catalyst preloaded Fenton oxidation combined with high-pressure homogenization method, starting from dissolved slurry. Then, using the hydrogen bonds and aldehyde bonds between F-CNF and PVA molecules, F-CNF/PVA composite films were prepared by solution casting method. Finally, the micro morphology of F-CNF, the distribution of F-CNF in polymer matrix, optical characteristics, chemical structure, and thermal stability of composite films were analyzed using SEM, AFM, CLSM, FTIR; the mechanical properties were tested by universal mechanical testing machine; swelling experiments, thermogravimetric analysis etc. – all of which provided basic theoretical and experimental data support for establishing an environmentally friendly high-performance green composite material preparation technology for F-CNF/PVA.

2 Experimental

2.1 Experimental raw materials

We used Hardwood Dissolved Pulp (Celgar Pulp Company, Canada); Ferrous sulfate heptahydrate, hydrogen peroxide (30% concentration), analytical grade (Tianjin Jiangtian Chemical Co., Ltd.); Polyvinyl alcohol (alcoholysis degree of 87-89 mol%), propylene glycol, analytical grade (Shanghai Aladdin Biochemical Technology Co., Ltd.); Rhodamine B thiocyanate, analytical grade (China National Pharmaceutical Group Chemical Reagent Co., Ltd.). All reagents are analytical grade and have not been further purified before use.

2.2 Experimental instruments

The following equipment were used in our experiments: 2500-II KRK high concentration disc grinder, KRK Corporation, Japan; AH-PILOT2015 High Pressure Homogenizer, Anteos Nanotechnology Co., Ltd., Canada; JSM-IT300 scanning electron microscope, Japan Electronics Corporation; D3100 Atomic Force Microscope, Veeco Corporation, USA; Leica TCA SP5 Laser Confocal Microscope, Leica GmbH, Germany; Vertex 70 Fourier Transform Infrared Spectrometer, Bruker GmbH, Germany; CMT4204 Universal Mechanics Testing Machine, Shenzhen Xinsansi Material Testing Co., Ltd; UV-3600 UV Visible spectrophotometer, Shimadzu Enterprise Management (China) Co., Ltd; STD 650 synchronous thermal analyzer, TA instrument from the United States; RW 20D cantilever mixer, IKA GmbH, Germany; HE83/02 Rapid Moisture Analyzer, Mettler Toledo Instruments (Shanghai) Co., Ltd.

2.3 Preparation of Fenton Oxidized Cellulose Nanofibers (F-CNF)

After preliminary mixing 200g of dissolved pulp (absolutely dry) and 0.03g/g of ferrous sulfate (based on dry fiber mass), the pulp concentration is adjusted to 25%, and quickly added it to the KRK refiner. The gap between the grinding discs is set at 0.5 mm and the slurry is cyclically stirred three times to ensure that Fe^{2+} enters the interior of the fibers and forms a "Fe^{2+}-fiber" composite catalytic system with cellulose macromolecules. Subsequently, the composite catalyst is transferred to a polyethylene self sealing bag, 0.08 g/g H_2O_2 (based on dry fiber mass) is added, and the reaction is carried out in a water bath at 45 °C for 60 minutes. After repeatedly washing the slurry with ionic water until the filtrate becomes neutral, the slurry concentration is adjusted to 1%, homogenized it at 60 MPa for 15 cycles, the prepared F-CNF is collected and cooled in a refrigerator for storage.

2.4 Preparation of F-CNF/PVA Composite Materials

2.4.1 Preparation of PVA aqueous solution

200 g of PVA particles and 800 g of deionized water are accurately weighed. A small amount of PVA is slowly added into deionized water several times, stirred in a water bath at 90 °C for 2 hours, and a 20% (w/w) PVA solution is prepared. It is cooled to room temperature and refrigerated at 5 °C for later use.

2.4.2 Preparation of F-CNF/PVA Composite Film

Accurately weighed 25 g of PVA solution with a concentration of 20% was added to a certain amount of F-CNF suspension and 0.15 g of propylene glycol, deionized water to 50 g is added and the pH of the solution is adjusted to 5 with sulfuric acid, sealed with the plastic film with magnetic stirring at 60 °C for 1 hour, centrifuged at 3000 r/min for 1 minute, and ultrasonically degassed for 5 minutes to obtain mixed solutions of composite materials with different amounts of added F-CNF. They are poured into a mold and dried in an oven at 40 °C for 12 hours to obtain F-CNF/PVA composite film.

2.5 F-CNF morphology and structural characterization

2.5.1 Scanning Electron Microscope (SEM)

F-CNF obtained by high-pressure homogenization was diluted to a certain ratio, ultrasonicated for 10 minutes to ensure uniform distribution, and freeze-dried. Subsequently, the freeze-dried sample was attached to the sample stage using conductive adhesive, and after gold spraying treatment, the microstructure of the nanofibers was observed using a JSM-IT300 scanning electron microscope. The Image J software was used to analyze scanning electron microscopy images and the size distribution and average diameter of F-CNF were determined.

2.5.2 Atomic Force Microscopy (AFM)

The F-CNF suspension obtained by high-pressure homogenization is diluted with alcohol to 0.005 wt%, after which the sample is air-dried on a clean mica plate using a dropper. Imaging was performed using a Veeco D3100 atomic force microscope in tap mode.

2.5.3 Infrared spectroscopy (FT-IR) analysis

The dry test sample and potassium bromide are weighed in a ratio of 1:100, crushed and pressed into transparent thin films, the scanning range is set to 4000–500 cm^{-1}, and the resolution is 4 cm^{-1}. A Fourier transform infrared spectrometer (VERTEX 70) is used to scan and determine the changes in F-CNF functional groups before and after oxidation.

2.5.4 Determination of carboxyl and aldehyde content

The changes in the carboxyl and aldehyde content of F-CNF before and after Fenton oxidation were determined using conductivity titration method [11].

2.6 Characterization of Structure and Properties of F-CNF/PVA Composite Materials

2.6.1 Scanning Electron Microscope (SEM)

The composite film (surface direct sampling, cross-section liquid nitrogen brittle fracture sampling) is attached to the sample stage with conductive adhesive, treated with gold sputtering, and the surface and cross-sectional microstructure of the F-CNF/PVA composite film is examined using a JSM-IT300 scanning electron microscope.

2.6.2 Laser confocal microscope (CLSM)

According to the method proposed by Dong S. et al. [14], Rhodamine thiocyanate B was grafted onto the surface of F-CNF using a three-step method. The distribution and aggregation of F-CNF in PVA were detected using a confocal laser microscope based on the phenomenon of red fluorescence generated at an excitation wavelength of 543 nm.

2.6.3 Tensile performance testing

According to GB/T1040–1992, the tensile properties of the F-CNF/PVA composite film were tested at room temperature using CMT4204 electronic universal mechanical testing machine. The width of the narrow part of the dumbbell shaped sample was 4.4 mm, the gauge length was 25 mm, and the loading speed was 50 mm/min. The average value was taken after 5 tests per group.

2.6.4 Optical performance testing

The F-CNF/PVA composite film was cut into 4 cm × 1 cm samples, and a UV-3600 UV visible spectrophotometer was used to measure the transmittance of the composite film within the wavelength range of 200-800 nm. Measure each sample three times and take the average.

2.6.5 Swelling performance testing

The 2cm×2cm F-CNF/PVA composite film was dried at 105 °C for 24 hours, then placed it in a closed environment with 98% RH (self-made saturated copper sulfate solution) for a certain period of time, and the change in the mass of the composite film after moisture absorption was observed. The swelling water

absorption rate of the sample was calculated according to formula (1). Three measurements per group were carried out and the average value was taken.

$$W = \frac{m_2 - m_1}{m_1} \times 100\% \quad (1)$$

In the formula, W represents the water absorption rate of the composite film (%); m_2 represents the mass of the composite film after moisture absorption in a high humidity environment (g); m_1 represents the initial mass of the composite film after drying (g).

2.6.6 Infrared Spectroscopy (FTIR) Analysis

After drying the test sample and spectroscopically pure potassium bromide at 105 °C for 4 hours, the sample was ground and compressed at a ratio of 1:100. The sample was scanned and measured on a VERTEX 70 Fourier transform infrared spectrometer to determine the changes in functional groups before and after moisture absorption. The scanning range was 4000–400 cm^{-1}, resolution 4 cm^{-1}, 32 scanning cycles.

2.6.7 Thermogravimetric analysis (TGA)

An STD 650 thermogravimetric analyzer was used to analyze the thermal stability of the test sample. Weighed 5 to 8 mg of the sample were placed it in an alumina crucible. Under nitrogen protection, the temperature was increased from 25 °C to 600 °C at a rate of 10 °/min, with a ventilation rate of 25 ml/min.

*2.6.8 Soil Burial Degradation Rate Tes*t

The 3 cm × 3 cm F-CNF/PVA composite film was dried at 80 °C until it reached constant weight and then placed in an equidistant soil pit in the meadow with a depth of 10 cm. After two weeks, the sample was taken out, wipe cleaned, dried for 2 hours, and the change in mass of the composite film was observed. The soil burial degradation rate of the sample is calculated according to formula (2). Three measurements per group were performed and the average value was taken.

$$W = \frac{m_0 - m_n}{m_0} \times 100\% \quad (2)$$

In the formula, W represents the soil burial rate of degradation of the composite film (%); m_0 represents the initial mass of the composite film after drying (g); m_n represents the mass of the sample after being buried in the soil for two weeks (g).

3 Results

3.1 F-CNF morphology and structural characterization

In the high shear catalyst preloading Fenton oxidation process, we consider a single fiber as a "microreactor" and use the method of high shear catalyst preloading to load Fe^{2+} onto the fiber cell wall during high concentration slurry grinding, forming a "Fe^{2+}- fiber" composite catalytic system [15]. Subsequently, hydrogen peroxide was introduced into the system under high concentration reaction conditions to maximize the confinement of the Fenton reaction within the microreactor, avoiding ineffective decomposition of hydrogen peroxide outside the fibers and improving the Fenton oxidation efficiency.

The SEM image of F-CNF after high-pressure homogenization, AFM image, the diameter distribution and FTIR spectrum are shown in Figure 1. As shown in Figure 1 (a) and (c), F-CNF prepared by catalyst preloading Fenton oxidation pretreatment and high-pressure homogenization exhibits a soft fibrous shape with diameters mostly in the range of 40–100 nm (accounting for 73.2%), an average diameter of 72.35 nm, and a length of tens or even hundreds of micrometers, with a high aspect ratio. The AFM image shows that the diameter of F-CNF is in the nanoscale range in Figure 1(c). The uniform nanoscale distribution and high aspect ratio provide certain performance guarantees for the application of F-CNF in the field of nanocomposite reinforcement materials.

Compared with the dissolution slurry, F-CNF showed a new carbonyl peak at 1734 cm^{-1} [16] in Figure 1(d), indicating that the hydroxyl groups of cellulose nanofibers were partially oxidized to aldehyde or carboxyl groups after Fenton oxidation. The conductivity titration results showed that the carboxyl and aldehyde groups in F-CNF were 83.46 μmol/g and 58.71 μmol/g, respectively, which increased the electrostatic repulsion between fibers and facilitated their dispersion in the polymer matrix.

3.2 Characterization of Structure and Properties of F-CNF/PVA Composite Materials

3.2.1 Microscopic morphology analysis of F-CNF/PVA composite film

The average thickness of the F-CNF/PVA composite film prepared by solution casting method is 88.73 μm. Figure 2 shows SEM images of the surface and cross-section of PVA

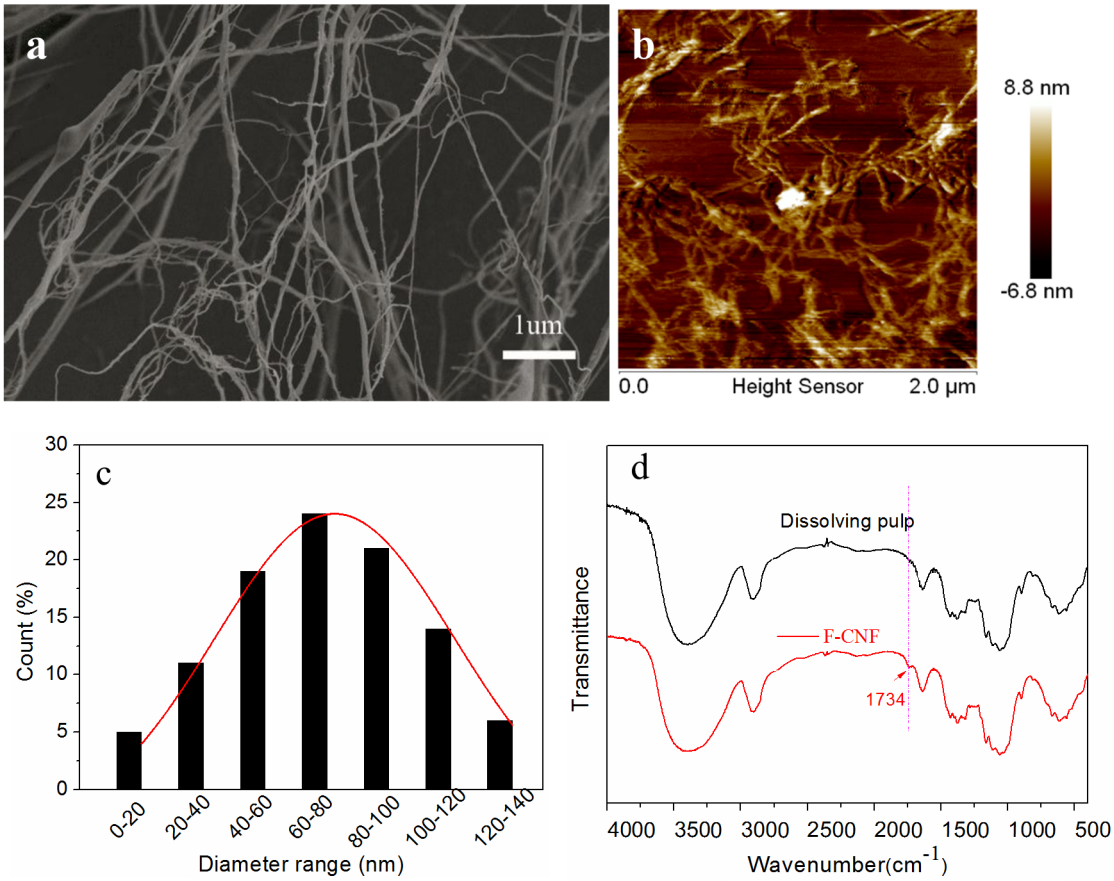

Fig. 1. Scanning Electron Microscopy (a), AFM (b), Diameter Distribution (c), and FTIR (d) of CNF

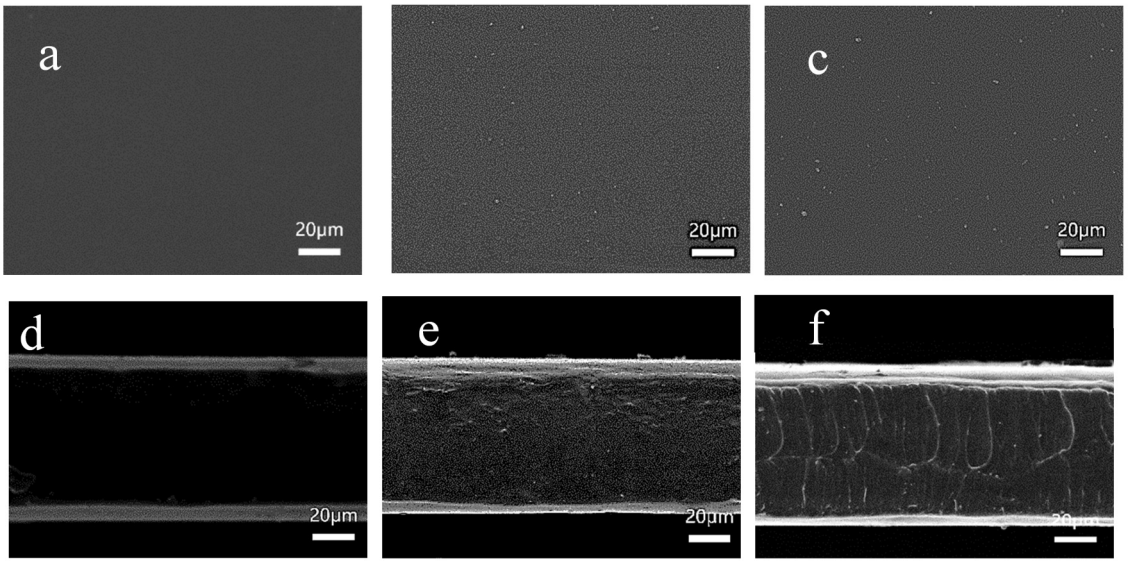

Fig. 2. SEM images of the surface (a, b, c) and cross-section (d, e, f) of PVA and F-CNF/PVA composite materials: (a), (d) F-CNF added at 0%; (b), (e) the addition amount of F-CNF is 10%; (c), (f) F-CNF addition amount is 20%

and typical F-CNF/PVA nanocomposite films. As shown in Figures 2 (a) and (d), the surface and cross-sectional structure of the pure PVA film are uniformly smooth and free of impurities. When 10% F-CNF was added, a small amount of white particles appeared on the surface of the composite film, and the cross-section became slightly rough (Figure 2b-e). With the addition of 20% F-CNF, the aggregation of white particles on the surface of the

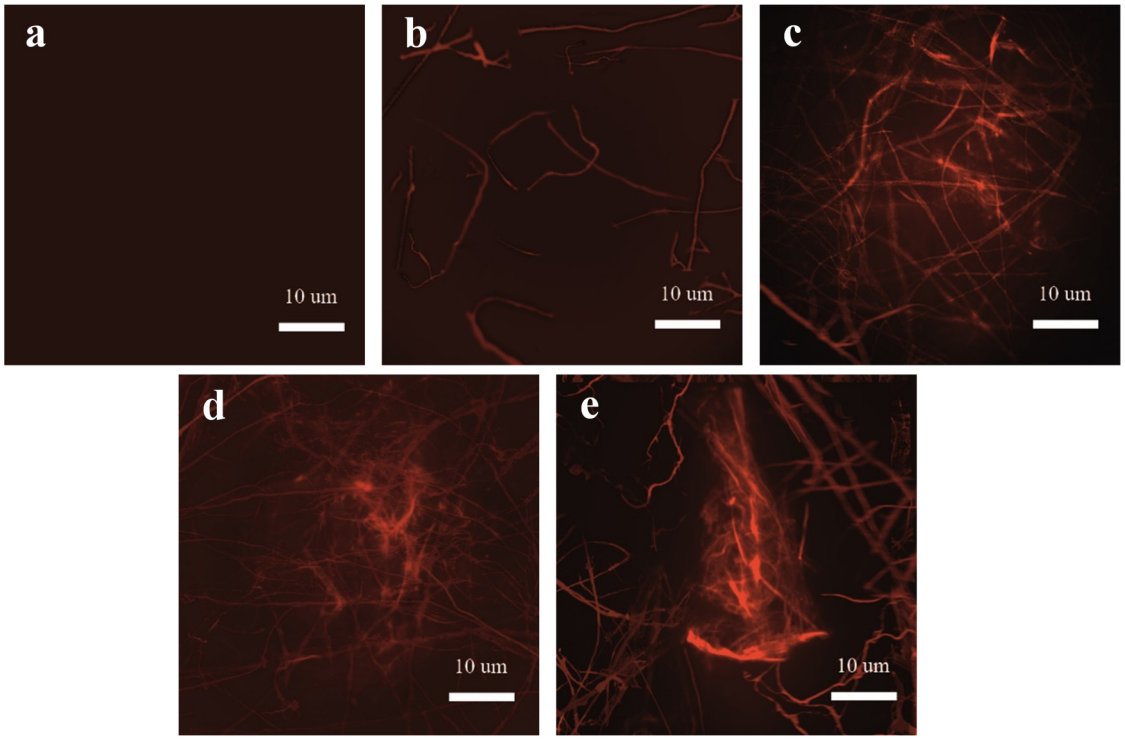

Fig. 3. Laser confocal microscopy image of the distribution of F-CNF in the composite film: (a) 0% F-CNF added; (b) the amount of F-CNF added is 5%; (c) the amount of F-CNF added is 10%; (d) the amount of F-CNF added is 15%; (e) the amount of F-CNF added is 20%

composite film becomes more obvious, the number of cross-sectional defects increases, and obvious fracture F-marks and wrinkles can be observed in Figure 2 (c) and (f). This indicates that with increasing addition of F-CNF, intensive stirring can no longer uniformly disperse it in the polymer matrix. Some nanofibers undergo self aggregation due to the nanoscale effect (high specific surface area and surface energy), forming fiber bundles or flocs distributed in the PVA composite film.

3.2.2 Dispersion analysis of F-CNF in F-CNF/PVA composite film

After grafting rhodamine B thiocyanate onto the surface of F-CNF, red fluorescence can be generated at an excitation wavelength of 543 nm. This property can be used to observe the distribution of F-CNF in the PVA matrix using laser confocal microscopy. Figure 3 shows laser confocal microscopy images of several typical F-CNF distributions in PVA. From Figure 3 (b) and Figure 3 (c), it can be seen that with the addition of 5% and 10% F-CNF, the nanofibers are uniformly dispersed in the PVA matrix, and the compatibility between the two is good. As the amount of added F-CNF increases, when the F-CNF content in the composite film is 15%, the fibers undergo local entanglement and aggregation in the matrix, and larger aggregated fiber bundles can be observed in Figure 3(d). With the addition of 20% F-CNF, the agglomeration phenomenon of fibers becomes more pronounced in Figure 3(e).

Table 1. Allocation of Infrared Spectral Absorption Bands

Wave number cm^{-1}	Absorption band attribution
3457	-OH stretching vibration (F-CNF, PVA)
2909	-CH stretching vibration (F-CNF, PVA)
1745	-C=O stretching vibration (F-CNF, PVA)
1635	The stretching vibration peak of H-O-H groups absorbing water (F-CNF, PVA)
1386	-CH bending vibration (F-CNF, PVA)

3.2.3 Chemical Structure Analysis of F-CNF/PVA Composite Membrane

Figure 4 shows the infrared spectra of F-CNF, PVA, and F-CNF/PVA composite films with different amounts of F-CNF added. Table 1 lists the main infrared characteristic absorption peaks of F-CNF and PVA. As shown in the figure, F-CNF and PVA exhibit typical -OH stretching vibration absorption peaks,

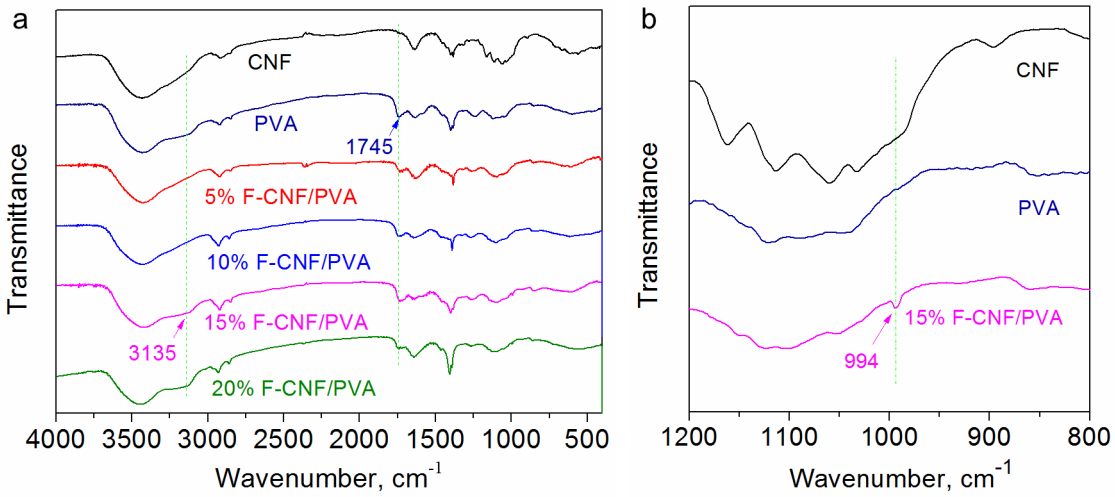

Fig. 4. Infrared spectra of CNF, PVA, and F-CNF/PVA composite materials

C-H stretching vibration peaks, stretching vibration peaks absorbing water H-O-H groups, and C-H bending vibration peaks originating from cellulose and polyvinyl alcohol at 3457 cm^{-1}, 2909 cm^{-1}, 1635 cm^{-1}, 1386 cm^{-1}, respectively [17–18]. In addition, PVA exhibits a C=O stretching vibration absorption peak at 1745 cm^{-1}, which is caused by incomplete alcoholysis during PVA preparation and the presence of residual carbonyl groups in the molecular chain [19].

As shown in Figure 4 (a), with the increase of F-CNF addition, the absorption peak between 3650-3000 cm^{-1} representing hydrogen bonds in the composite material widens and gradually shifts towards lower wavenumbers, and typical characteristic absorption peaks representing intermolecular hydrogen bonds are split at 3135 cm^{-1} [20-23]. Research has shown that the hydroxyl stretching vibration absorption peaks of F-CNF and PVA include the superposition of vibrations of free hydroxyl groups, bound hydroxyl groups, and intermolecular bound hydroxyl groups in the molecule, forming a relatively dispersed broad peak [19, 22-23]. After combining these two groups, a large number of -OH, -COOH and C-O-C can form intermolecular hydrogen bonds with -OH of PVA, greatly increasing the proportion of intermolecular hydrogen bonds in the composite material. The larger the amount and more uniform the distribution of F-CNF, the stronger the intermolecular hydrogen bond binding between the two, resulting in the enhancement and separation of the absorption peak representing intermolecular hydrogen bonds in the infrared spectrum. This phenomenon indicates that there is a strong hydrogen bonding interaction between F-CNF and PVA molecules, and they are well compatible.

By comparing the infrared curves of F-CNF, PVA, and composite films, it can be seen that the infrared spectrum of F-CNF/PVA composite film shows an aldehyde ring absorption peak at 994 cm^{-1} [24-25] (Figure 4b), indicating that the aldehyde group in the F-CNF molecular chain undergoes an aldehyde crosslinking reaction with the hydroxyl group of PVA, which is beneficial for improving the comprehensive properties of the composite material.

3.2.4 Analysis of Mechanical Properties of F-CNF/PVA Composite Membrane

Figure 5 shows the tensile performance curves of F-CNF/PVA composite films with different amounts of cellulose nanofibers added. As shown in the figure, when the amount of F-CNF added is 0, the tensile strength of the pure PVA film is 20.54 MPa and the elastic modulus is 156.97 MPa. With the increase of F-CNF added, the tensile strength and elastic modulus of the composite film rapidly increase. With the addition of 15% F-CNF, the tensile strength of the composite film is 65.27 MPa, and the elastic modulus is 1460.32 MPa, which is 217.77% and 830.69% higher than that of pure PVA. After that, as the addition of F-CNF continued to increase, the tensile strength and elastic modulus of the composite film showed a relatively gentle growth trend.

Due to its nanoscale effect, CNF has extremely high strength and Young's modulus. According to the ROM addition theory of composite material reinforcement, adding it to the polymer matrix can significantly improve the

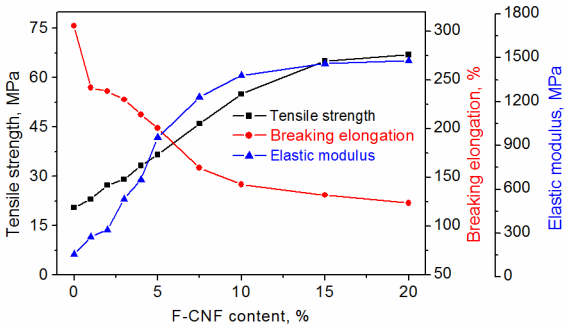

Fig. 5. Tensile Properties of F-CNF/PVA Composite Materials

mechanical properties of the composite material, and the degree of reinforcement is closely related to the dispersibility of CNF in the polymer matrix and the interfacial compatibility between them [26-27]. Both F-CNF and PVA molecular chains contain a large amount of -OH, which is easy to form hydrogen bonds. The compatibility between the two phases is good, and the nanofibers can be evenly distributed in the PVA matrix. The large aspect ratio of F-CNF enables them to interweave and wrap around each other in the polymer matrix to form a unique three-dimensional network structure shown in Figure 3(c) and (d), which can better achieve the transmission and diffusion of external loads [28-30] and is more conducive to the improvement of the mechanical properties of composite materials. However, when the amount of F-CNF added was too large (20% in this study), the aggregated nanofibers shown in Figure 3(e) had limited effect on improving the mechanical properties of the composite material and even caused a decrease in performance. While the tensile properties of the composite material are improved, due to the rigidity of F-CNF and its limiting effect on the movement of PVA molecular segments, the fracture elongation of the composite material significantly decreases with the increase of F-CNF addition (Figure 5). However, compared with the nanofiber/PVA composite material without propylene glycol plasticizer, it still exhibits higher flexibility [31-32].

3.2.5 Optical Performance Analysis of F-CNF/PVA Composite Film

Figure 6 shows the transmittance curves of PVA and F-CNF/PVA composite materials. As shown in the figure, the transmittance curves of composite films with different F-CNF addition amounts are very close. In the central part of the visible light range of 600 nm, the transmittance of PVA film is 90.23%, and the

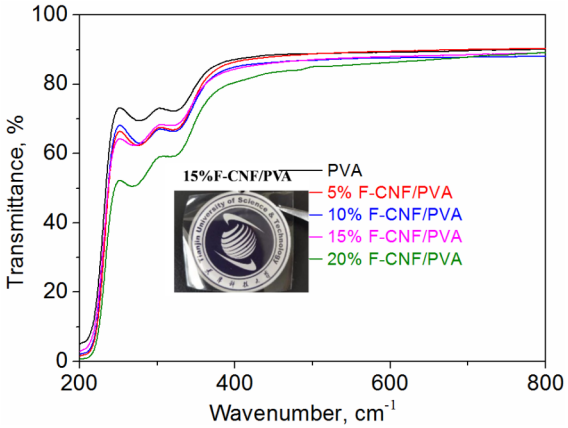

Fig. 6. Transmittance of PVA and F-CNF/PVA composite materials

transmittance of each composite film is also above 86.47%, indicating high transparency. Research has shown that when the diameter of nanofibers is less than 1/10 of the wavelength of visible light waves, light scattering can be effectively avoided, and the film materials prepared from it have high transmittance [33]. As mentioned earlier, the average diameter of F-CNF prepared by catalyst preloading and synergistic Fenton oxidation method is 68.32 nm. Therefore, adding it to PVA substrate will not have a significant impact on the transmittance of the composite material. As the amount of F-CNF added increases, the partial aggregation of nanofibers and the proportion of F-CNF greater than 1/10 of their wavelength in various wavelength ranges of visible light also increase, resulting in a decrease in the transparency of the composite film. However, overall, the transparency of each composite film is relatively high, and the addition of F-CNF has little effect on the transmittance of the composite film. With the addition of 20% F-CNF, the transmittance of the composite film at 600 nm is 86.47%, which is only 4.17% lower than that of the PVA film.

3.2.6 Analysis of Swelling Properties of F-CNF/PVA Composite Membrane

The water absorption swelling rate, as an important parameter of hydrophilic degradable composite materials, has a significant impact on the properties and application range of the composite materials. Figure 7 shows the water absorption and swelling curves of PVA and F-CNF/PVA nanocomposites. As shown in the figure, at 98% relative humidity, the swelling rate of each material rapidly increases with the increase of water absorption time. After 36 hours, the swelling curve rises slowly and gradually becomes flat. Compared with pure

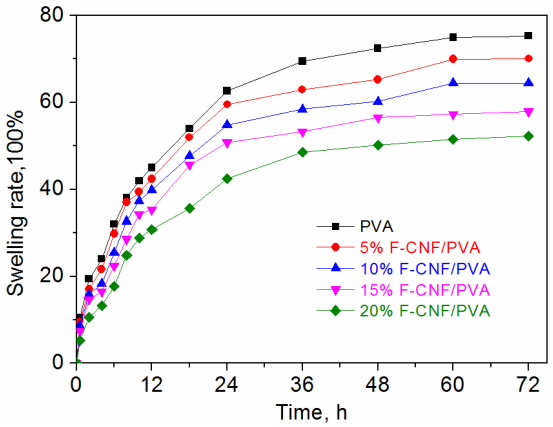

Fig. 7. Swelling curves of PVA and F-CNF/PVA composites

PVA film, the addition of F-CNF results in abundant -OH, -COOH and C-O-C groups interact with the hydroxyl groups on the PVA molecular chain, forming a large number of hydrogen bonds, and the occurrence of the interphase aldol reaction further reduces the interaction between PVA free hydroxyl groups and water molecules [24-25], thereby reducing the water absorption and swelling rate of the composite material. With the increase of F-CNF addition and the improvement of its dispersion uniformity in the PVA matrix, the swelling rate of the F-CNF/PVA composite material further decreases. With the addition of 15% CNF, the swelling rate of the composite membrane after 60 hours of water absorption and swelling is 56.23%, which is 24.92% lower than the 74.89% of the pure PVA membrane. Although SEM and CLSM results showed partial aggregation of F-CNF in the PVA matrix with 20% additive, the effect of aggregation on improving the swelling properties was smaller than the effect of increasing CNF content on decreasing the swelling properties. Therefore, the swelling rate of the composite material further decreased. The above results indicate that the addition of F-CNF can to some extent reduce the water absorption and swelling rate of the composite material, and the swelling rate of F-CNF/PVA composite film gradually decreases with the increase of CNF addition, expanding the application field of PVA nanocomposites in high humidity environments.

3.2.7 Thermal stability analysis of F-CNF/PVA composite film

The thermogravimetric (TG) and differential thermogravimetric (DTG) curves of PVA and F-CNF/PVA nanocomposites are shown in Figure 8. It can be seen from the figure that the thermal weight loss process of PVA and composite materials can be divided into three stages. In the first stage (30-280 °C), the weight loss is relatively slow, which is attributed to the evaporation of bound water and adsorbed water in the membrane material. In the second stage (280-400 °C), there is a rapid weight loss, during which the chains of polyvinyl alcohol and F-CNF macromolecules break and gradually decompose into small volatile substances that escape. The third stage (400-600 °C) is mainly the heat loss process of carbon containing substances, during which the material weight loss returns to a plateau.

Comparing the TG and DTG curves of various composite materials with pure PVA film, it can be seen that the initial thermal decomposition temperature and the maximum weight loss rate temperature of F-CNF/PVA nanocomposite materials have increased to a certain extent compared to pure PVA film, and the increase is more significant with the increase of F-CNF addition. This fully demonstrates that the ad-

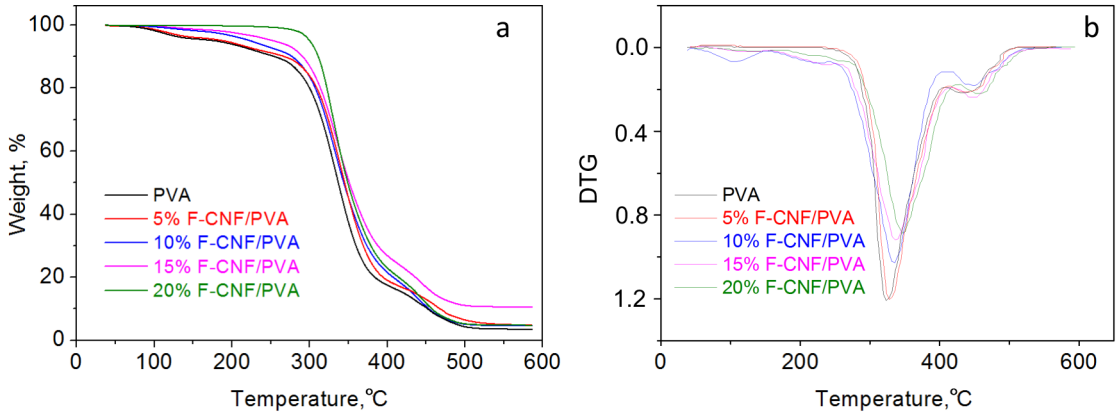

Fig. 8. TG (a) and DTG (b) curves of PVA and F-CNF/PVA composite materials

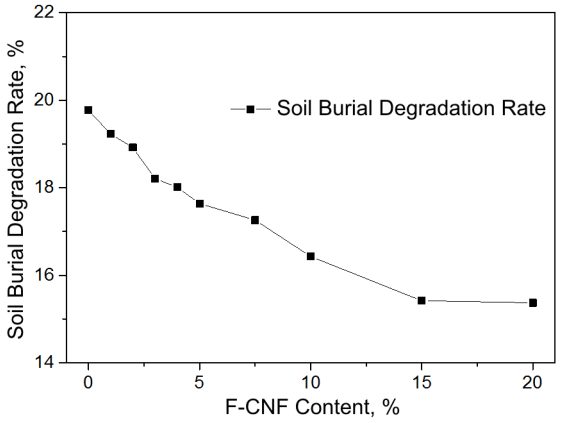

Fig. 9. Soil burial degradation rate of F-CNF/PVA composite films

dition of F-CNF to the PVA matrix improves the thermal stability of the composite material. This is due to the formation of hydrogen bonding and aldehyde crosslinking between F-CNF and PVA molecular chains, which is beneficial for improving the thermal stability of the composite material.

3.2.8 Soil burial degradation analysis of F-CNF/PVA composite film

As can be seen from Figure 9, in the natural soil environment, the composite film exhibits a good soil burial degradation performance, with its soil-burial degradation rate ranging from 14.68% to 18.88%. As the addition amount of F-CNF gradually increases, the soil-burial degradation rate shows a gradual downward trend. When the addition amount of F-CNF reaches 10%, the soil-burial degradation rate tends to be stable. This is because the addition of F-CNF promotes the formation of a denser structure in the composite film, thus reducing the penetration rate of microorganisms and further slowing down the biodegradation rate of the film. However, when the addition amount of F-CNF is too large, CNF aggregates in the PVA matrix, and its promoting effect on the formation of the dense structure of the composite film becomes limited.

4. Conclusions

(1) Fenton oxidized cellulose nanofibers (F-CNF) were prepared by catalyst preloading and Fenton oxidation pretreatment combined with high-pressure homogenization method. F-CNF/PVA composite films were prepared by solution casting method based on the construction of hydrogen bonds between F-CNF and PVA molecules.

(2) The SEM and CLSM results indicate that F-CNF can be uniformly dispersed in the PVA matrix, and both have good interfacial compatibility. As the amount of F-CNF added increases, some nanofibers undergo self aggregation due to the nanoscale effect, forming fiber bundles or flocs distributed in the PVA composite film.

(3) The FTIR results showed that a large number of hydrogen bonds were formed between F-CNF and PVA molecules, and an aldol reaction occurred. The results of stretching, swelling, thermal stability and biodegradability testing showed that the addition of F-CNF significantly improved the tensile strength and elastic modulus of the composite film, reduced its water absorption, improved its thermal stability and exhibited good soil burial degradation properties. When the addition amount of F-CNF was 15%, the tensile strength and elastic modulus of the composite film reached 65.27 MPa and 1460.32 MPa, respectively, which increased by 217.77% and 830.69% compared to the control group (100% PVA) sample, respectively. The improvement of the comprehensive performance of the F-CNF/PVA composite film has expanded its application value in the field of high-performance green composite materials.

Acknowledgment

This work is supported by the Science and Technology Innovation Plan Project of the Education Department of Shanxi Province (No. 2024L514).

References

1. O. Nechyporchuk, M. N. Belgacem, J.Bras, *Industrial Crops and Products*, **93**, 2, (2016).
2. ZHANG Sihang, FU Runfang, DONG Liqin, et al. *China Pulp Paper*, **36(1)**, 67, (2017)
3. M. Bulota, K. Kreitsmann, M. Hughes, et al. *Journal of Applied Polymer Science*, **126**, 448 (2012).
4. Azizi Samir MAS, F. Alloin, M. Paillet, et al., *Macromolecules*, **37**(11), 4313 (2004).
5. T. Zimmermann, E. Pöhler, T. Geig, *Advanced Engineering Materials*, **6**(9), 754 (2004).
6. T. Zimmermann, E. Pöhler, P. Schwaller, *Advanced Engineering Materials*, **7**(12), 1156, (2005).
7. L.I. Qun, WANG Aijiao, WANG Zehai.A Method for Preparation of Nanocellulose by Iiron-catalyzed Hydrogen Peroxide Oxidation.CN, 2017113435931.2018-01-01.

8. Q. Li, A.J. Wang, K.Y. Long, et al. *ACS Sustainable Chemistry & Engineering*, **23**(2), 1129, (2018).
9. D.F. Guay, B.J.W. Cole, R.C. Fort, et al., *Journal of Wood Chemistry and Technology*, **20**(4), 375, (2000).
10. D.F. Guay, B.J.W. Cole, R.C. Fort, et al., *Journal of Wood Chemistry and Technology*, , **21**(1), 67, (2001).
11. DUAN Lin-juan, DUAN Yan, M.A. Wei, et al. *China Pulp & Paper*, **39** (1), 9, (2020).
12. E. Fortunati, D. Puglia, M. Monti, et al., *Journal of Applied Polymer Science*, **128**(5), 3220, (2013).
13. A.J. Uddin, J. Araki, Y.Gotoh, *Biomacromolecules*, **12**(3), 617 (2011).
14. S. Dong, M. Roman, *Journal of the American Chemical Society*, **129**(45), 13810, (2007).
15. Duan Linjuan, Liu Rongrong, Li Qun, *Starch-starke*, **72**(11–12), 1900259, (2020).
16. HUANG Xiaolei, LIU Wen, LIU Qunhua, et al.China Pulp Paper, **34**(1), 18 (2015).
17. R.T. O'Connor, E.F. DuPré, D. Mitcham, *Textile Research Journal*, **28,** 382, (1958).
18. S. Ostovareh, K. Karimi, A. Zamani.*Industrial Crops and Products*, **66**, 170, (2015).
19. BAI Lu, ZHANG Li-Ping, QU Ping, et al. *Chemical Journal of Chinese Universities*, **32**(4), 984, (2011).
20. Chen Yangmei, Wang Yan, Ma Yongwen, et al., *Cellulose*, **17**(2), 329, (2010).
21. M. Schwanninger, J.C. Rodrigues, H. Pereirac, et al.*Vibrational Spectroscopy*, **36**, 23, (2004).
22. L.V. Hui-lin, M.A. Yong-wen, WAN Jin-quan, et al. *Transactions of China Pulp and Paper*, **26**(1), 1, (2011).
23. SangYoun Oh, Dong Il Yoo, Younsook Shinet, et al. *Carbohydrate Research*, **340**, 2376, (2005).
24. J. Wang, C. Gao, Y. Zhang, et al. *Materials Science & Engineering C*, **30**, 214, (2010).
25. L.E. Millon, C.J. Oates, W.K. Wan, *J Biomed Mater Res Part B: Appl Biomater*, **90B**(2), 922, (2009).
26. F. Vilaseca, J.A. Mendez, J.P. Lopez, et al., *Chemical Engineering Journal*, **138**(1), 586, (2008).
27. A. Kelly, W.R. Tyson, *Journal of the Mechanics and Physics of Solids*, **13**(6), 329, (1965).
28. Azizi Samir MAS, F. Alloin, M. Paillet, et al. *Macromolecules*, **37**(11), 4313, (2004).
29. T. Zimmermann, E. Pöhler, T. Geiger, *Advanced Engineering Materials*, **6**(9), 754. (2004).
30. T. Zimmermann, E. Pöhler, P. Schwaller, *Advanced Engineering Materials*, **7**(12), 1156, (2005).
31. V. Sanna V. Sauli H. Harri et al., *Cellulose*, **21**, 3561, (2014).
32. Q. Kaiyan N.N. Anil, *Composites Science and Technology*, **72**, 1588, (2012)
33. K. Abe S. IwamotoH. Yano, *Biomacromolecules*, **8**(10), 3276, (2007).